Macromolecules
ARTICLE

Macromolecules **2011**, *44*, 383–392 **383**
DOI: 10.1021/ma1020837

Simulating the Relaxation of Stretched DNA in Slitlike Confinement

Daniel W. Trahan and Patrick S. Doyle*

Department of Chemical Engineering, Massachusetts Institute of Technology, Cambridge, Massachusetts 02139, United States

Received September 8, 2010; Revised Manuscript Received November 27, 2010

ABSTRACT: Brownian dynamics simulations of bead−spring chains were used to study the relaxation of an initially stretched DNA molecule in slitlike confinement. Taking into account excluded volume effects but neglecting hydrodynamic interactions, the simulations are able to reproduce the two relaxation times in the linear force regime that our group has experimentally studied and recently reported. The relaxation dynamics of the transverse dimensions are extensively studied, and a theoretical model is developed to describe them. The interplay between the longitudinal and the transverse dynamics is investigated and used to corroborate a physical model previously proposed to describe polymer relaxation in a slit.

1. Introduction

1.1. Motivation. The emergence of micro- and nanofluidic devices has led to many new and exciting developments in the field of single-molecule manipulations. For example, DNA separations[1,2] and genomic mapping[3,4] have benefited greatly from the precise control offered by so-called "lab-on-a-chip" devices. More generally, these microscopic systems have provided an important new platform to study fundamental problems in polymer physics.[5−11]

One recent problem that has received a considerable amount of attention is the relaxation dynamics of DNA in different types of confined environments.[6,10,12,13] This is particularly important for many single-molecule mapping devices that rely upon collisions[14] and field gradients[3,14] to deform DNA for subsequent analysis. This deformation process is highly dependent upon the balance between the stretching rate of the device and the relaxation of the polymer. Therefore, understanding how confinement affects the relaxation process of confined polymers is critical both to optimizing current technologies and to developing novel device designs.

Additionally, many important biological molecules are polymeric in nature (e.g., DNA, actin, and microtubules, although only DNA is typically flexible enough and of sufficient length to observe the sort of relaxation processes we shall study), and most cellular environments are highly confined. For example, 3 m of human DNA is packed into a nucleus of around 5 μm in diameter. Study of the dynamics of confined DNA molecules is critical to understanding how the cell stores, accesses, and replicates its genetic information. In vivo relaxation of chromosomal DNA has even been used to probe the intracellular environment.[15]

1.2. Past Work. Over the last two decades, the relaxation of unconfined polymers has been studied comprehensively both experimentally[5] and via simulations.[16−18] They have confirmed the theoretical prediction that unconfined single molecule relaxation is well-described by a single longest relaxation time τ_I over all extensions within the chain's linear force regime[19] (from equilibrium to ∼30% fractional extension[5]). However, relaxation in slitlike confinement has been studied much less extensively, with several studies offering contradictory findings.[6,13,20−23] It is only recently that these results have begun to be reconciled by suggesting the existence of two relaxation times in the linear force regime.[10]

The dynamics of polymers in slitlike confinement were first treated theoretically by Brochard[24] using blob theory. The first direct observation of such confined relaxation, by Bakajin and co-workers,[6] was of molecules relaxing after having been highly stretched by collisions with microfabricated posts. The results produced scalings for the relaxation time that were more in line with the unconfined case.[10] Nearly a decade later, new experiments from our group obtained the confined relaxation time by measuring the rotational autocorrelation function of chains at equilibrium.[13] This study found good agreement with the blob theory predictions, contradicting the previous work of Bakajin et al.[6] Interestingly, several simulation studies found evidence to support the findings of both of the aforementioned experimental works. Simulating the relaxation of initially stretched chains[22,23] reproduced the un-confined-like results of Bakajin et al.,[6] while Monte Carlo simulations of chains at equilibrium[20,21] corroborated the blob theory scalings seen by our group.[13]

Although seemingly contradictory, taken together these studies hint at the cause of the discrepancies. All the work where chains were perturbed from equilibrium agree with each other and demonstrate un-confined-like behavior. On the other hand, agreement was also seen among the studies of chains at equilibrium which exhibited blob scalings. To explain this, our group suggested that two distinct relaxation times existed in the linear force regime.[10] When the molecule is stretched, the width of the chain in the transverse dimension is smaller that the height of the channel, and the confining walls do not significantly affect the conformation of the molecule. Therefore, the chain is governed by an un-confined-like relaxation time τ_I. However, at or near equilibrium, the polymer feels the full steric effects of the confining walls, and its dynamics slow as a consequence. A second relaxation time τ_{II} emerges which is longer than τ_I and which follows the predictions of blob theory.

Our group has shown that both of these relaxation times can be seen and measured by observing the longitudinal relaxation of initially stretched molecules over time scales

*To whom correspondence should be addressed. E-mail: pdoyle@mit.edu.

Published on Web 12/21/2010

long enough for the chain to reach equilibrium.[10,25] A physical model based upon blob theory has also been proposed that assumes this extension-dependence of the relaxation time is due entirely to excluded volume effects (EV) and not hydrodynamic interactions (HI). Although there is some experimental evidence that this model is correct, experiments are greatly hampered by the fact that the dynamics cannot be accurately measured on small time and length scales, especially in the dimension transverse to the plane of the channel.

1.3. Problem Statement. In this paper, we study the relaxation of a bead−spring chain in slitlike confinement from a stretched configuration that is initially straight using a combination of simulations and theory. Because simulations allow us to set which physics will be included, we can conclusively determine if excluded volume effects are sufficient to reproduce the qualitative features observed in experiments (e.g., two relaxation times). In addition, simulations can probe dynamics of the relaxation process on length and time scales that are inaccessible to experiments, particularly in the confined dimension. This allows us to consider the interplay between the dynamics in the direction of initial stretch and the confined dimension, enabling us to assess the validity of the current physical model for confined relaxation and its underlying assumptions.

2. Background

We now describe the theory of polymer relaxation both unconfined and in slitlike confinement. We start by considering the equilibrium size of a polymer chain and the basics of blob theory. We then use these results to develop scalings for the relaxation times of these chains. We also explain the current physical model of relaxation in slitlike confinement and some of its consequences.

In particular, we concern ourselves with the expected theoretical scalings based upon the physics included in our simulations. Therefore, we take EV into account, but we neglect the effects of HI. The chains are assumed to be free-draining so that

$$\zeta = N_K \zeta_K \tag{1}$$

where ζ and ζ_K are the chain and Kuhn length drag coefficients, respectively. Additionally, HI with the channel walls is neglected, and changes in the chain diffusivity due to confinement are ignored. Intramolecular HI decreases the relaxation time and affects the scaling of the relaxation time with chain length for an unconfined chain, while HI with channel walls increases the relaxation time and affects its scaling with channel height. However, we are unconcerned with these physics in this work and wish to isolate the effects of EV on the relaxation time in confinement.

2.1. Equilibrium Chain Size. The polymer is modeled as a chain composed of N_K Kuhn steps each of length b_K. When unconfined, the equilibrium radius of gyration $R_{g,0}$ of the chain can be determined from the statistics of random walks

$$\frac{R_{g,0}}{b_K} \sim {N_K}^{\nu_{3D}} \tag{2}$$

where ν_{3D} is the scaling exponent for the equilibrium chain size in a 3D environment. If the chain is ideal and intramolecular excluded volume effects are neglected, then $\nu_{3D} = 1/2$. The inclusion of EV causes the chain to swell and increases the scaling exponent to $\nu_{3D} \approx 3/5$.

In slitlike confinement, the polymer is squashed like a pancake, and due to EV, it swells in size even further. Blob theory is often used to describe confined polymers.[26] In this framework, the polymer is represented by a string of N_K/g blobs, where g is the number of Kuhn segments per blob

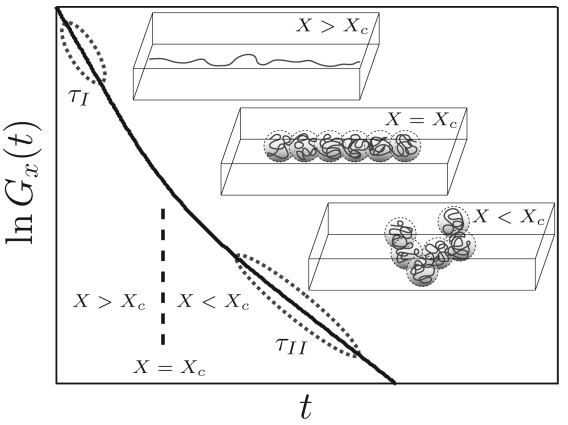

Figure 1. A cartoon depicting the physical model of confined relaxation based upon tension-blobs and how it relates to the longitudinal relaxation function $G_x(t) = \langle X(t)^2 \rangle - \langle X_{eq}{}^2 \rangle$, where $X(t)$ is the fractional extension in the longitudinal direction and X_{eq} is its average equilibrium value. Above a certain crossover extension X_c, the chain is not sterically confined and relaxes as if it were unconfined. Below X_c, the confining walls become important, and the chain relaxes by rearranging its self-avoiding blobs.

(see Figure 1). The size of a blob is set by the height of the channel, h.

On length scales smaller than h (i.e., within a blob), the polymer retains its un-confined-like behavior. So using eq 2, we can say that $h \sim g^{\nu_{3D}} b_K$, and upon rearrangement, the number of Kuhn segments g in a blob is given by

$$g \sim \left(\frac{h}{b_K}\right)^{1/\nu_{3D}} \tag{3}$$

On scales larger than h, the blobs, which repel each other due to EV, obey the scalings of a 2D self-avoiding walk (2D-SAW). So in slitlike confinement, the size of the chain is given by

$$\frac{R_{g,0}}{b_K} \sim \left(\frac{N_K}{g}\right)^{\nu_{2D}} \frac{h}{b_K} \sim {N_K}^{\nu_{2D}} \left(\frac{h}{b_K}\right)^{1-\nu_{2D}/\nu_{3D}} \tag{4}$$

where $\nu_{2D} = 3/4$.

2.2. Relaxation Times. *2.2.1. Unconfined.* First, we consider the relaxation of an unconfined linear polymer. Scalings for the longest relaxation time of the chain can be derived by considering a force balance between the elastic spring force F_E of the chain and the drag force F_D that opposes it. The force required to stretch a chain away from its equilibrium size R_0 by an amount δR is given by

$$F_E \sim -\frac{k_B T}{{R_0}^2} \delta R \tag{5}$$

where k_B is the Boltzmann constant and T is the temperature. Note that, from a scaling perspective, R_0 can be any measure of the equilibrium size of the coil, including the radius of gyration $R_{g,0}$ or the end-to-end distance $R_{ee,0}$. The drag force felt by the chain is

$$F_D \sim -\zeta \dot{R} \tag{6}$$

where $\dot{R}$ is the rate of change of the size of the chain. Balancing these forces gives the longest relaxation time τ_I for the chain

$$\tau_I \sim -\frac{\delta R}{\dot{R}} \sim \frac{\zeta {R_0}^2}{k_B T} \tag{7}$$

Introducing the results from eqs 1 and 2 and noting that $\zeta_K = k_B T/D_K$, we arrive at

$$\frac{\tau_I}{{b_K}^2/D_K} \sim {N_K}^{1+2\nu_{3D}} \tag{8}$$

where D_K is the diffusivity of a Kuhn segment.

2.2.2. Slitlike Confinement. When a molecule in a slit is stretched strongly enough, it is not sterically confined by the walls of the channel (see Figure 1). Therefore, the initial relaxation process is unaffected by the presence of the confining walls, and the molecule relaxes with the un-confined-like time constant τ_I given by eq 8. However, as the molecule relaxes, its lateral dimensions grow in size, and the confining effects of the wall become significant. This slows down the relaxation process, and a new, longer relaxation time τ_{II} emerges that governs the remaining relaxation to equilibrium.

A simple physical model based upon a quasi-steady tension-blob framework was proposed by Balducci and co-workers[10] to describe the transition between these two relaxation times. The stretched molecule can be represented by a string of N_K/g tension-blobs[27] of size ξ, where g is again the number of Kuhn segments per blob. Unconfined scalings hold within each blob so $g \sim (\xi/b_K)^{1/\nu 3D}$. The fractional extension of the chain X is then given by $X = \xi/gb_K \sim (\xi/b_K)^{1-1/\nu_{3D}}$. If the crossover from τ_I to τ_{II} occurs when the tension-blob size reaches the height of the channel (i.e., $\xi = h$), then the critical fractional extension X_c at which this crossover occurs is given by

$$X_c \sim (h/b_K)^{1-1/\nu_{3D}} \tag{9}$$

Above X_c, the molecule relaxes by growing the size of the tension blobs. But below X_c, tension-blob growth is restricted by the confining walls, and the molecule relaxes by rearranging the blobs. An interesting consequence of this model is that X_c is independent of chain length.

To determine τ_{II}, we employ eq 7 which is valid near equilibrium. We simply use the blob scalings for $R_{g,0}$ as given in eq 4. At or near equilibrium, the relaxation time of a confined molecule is given by

$$\frac{\tau_{II}}{{b_K}^2/D_K} \sim {N_K}^{1+2\nu_{2D}} \left(\frac{h}{b_K}\right)^{2(1-\nu_{2D}/\nu_{3D})} \tag{10}$$

3. Simulation Method

We simulated the relaxation of DNA using a model developed by Kim and Doyle.[28] This method is based upon Brownian dynamics and is well-suited for studying the dynamics of DNA in microfludic devices. A brief description of the numerical model is presented here.

3.1. Brownian Dynamics. DNA molecules are modeled as chains of N_b beads connected by $N_s = (N_b - 1)$ springs. The equation of motion for the position r_i of the ith bead is

$$\frac{d\boldsymbol{r}_i}{dt} = \frac{1}{\zeta_b}\left[\boldsymbol{F}_i^B(t) + \boldsymbol{F}_i^S(t) + \boldsymbol{F}_i^{EV}(t) + \boldsymbol{F}_i^{EV,\,wall}(t)\right] \tag{11}$$

where ζ_b is the bead drag coefficient, $\boldsymbol{F}_i^B$ is the Brownian force, $\boldsymbol{F}_i^S$ is the total spring force felt by the bead, $\boldsymbol{F}_i^{EV}$ is the intrachain excluded volume force due to nearby beads, and $\boldsymbol{F}_i^{EV,wall}$ represents the interaction of the bead with the wall of the device.

We nondimensionalize the variables as follows:

$$\hat{\boldsymbol{r}} \equiv \frac{\boldsymbol{r}}{l_s},\ \hat{t} \equiv \frac{t}{{l_s}^2/D_b} \tag{12}$$

where $\boldsymbol{r}$ is position, l_s is the maximum extension of a single spring ($l_s \equiv L/N_s$), t is time, and $D_b = k_B T/\zeta_b$ is the diffusivity of a bead.

We nondimensionalize the forces $\boldsymbol{F}$ as follows:

$$\hat{\boldsymbol{F}}(\hat{\boldsymbol{r}}) \equiv \frac{\boldsymbol{F}}{k_B T/l_s} \tag{13}$$

This leads to the nondimensional form of eq 11:

$$\frac{d\hat{\boldsymbol{r}}_i}{d\hat{t}} = \hat{\boldsymbol{F}}_i^B + \hat{\boldsymbol{F}}_i^S + \hat{\boldsymbol{F}}_i^{EV} + \hat{\boldsymbol{F}}_i^{EV,\,wall} \tag{14}$$

The nondimensional Brownian force is given by:

$$\hat{\boldsymbol{F}}_i^B = \sqrt{\frac{24}{\Delta\hat{t}}}\,(\boldsymbol{r}_n)_i \tag{15}$$

where $\Delta\hat{t}$ is the dimensionless time step and $(\boldsymbol{r}_n)_i$ are uniform random numbers such that each component $(\boldsymbol{r}_n)_i^j \in [-1/2, 1/2]$, where j denotes the coordinate x, y, or z. The net nondimensional spring force on the ith bead is

$$\hat{\boldsymbol{F}}_i^S = \begin{cases} \hat{\boldsymbol{f}}_{i,2}^s, & i = 1 \\ \hat{\boldsymbol{f}}_{i,i+1}^s + \hat{\boldsymbol{f}}_{i,i-1}^s, & 1 < i < N_b \\ \hat{\boldsymbol{f}}_{i,N_b-1}^s, & i = N_b \end{cases} \tag{16}$$

where the spring force $\hat{\boldsymbol{f}}_{i,j}^s$ is given by a spring law developed by Underhill and Doyle[29] to correctly reproduce the Marko-Siggia spring force law for a wormlike chain[30] at varying degrees of coarse-graining:[31]

$$\hat{\boldsymbol{f}}_{i,j}^s = v\left[\frac{1}{(1-\hat{r}_{j,i}^2)^2} - \frac{7}{v(1-\hat{r}_{j,i}^2)} + C + B(1-\hat{r}_{j,i}^2)\right]\hat{\boldsymbol{r}}_j - \hat{\boldsymbol{r}}_i \tag{17}$$

where v is the number of persistence lengths represented by each spring ($v \equiv l_s/A_p$), $\hat{r}_{j,i}$ represents the distance between $\hat{\boldsymbol{r}}_j$ and $\hat{\boldsymbol{r}}_i$, $C = 3/32 - 3/4v - 6/v^2$, and $B = (13/32 + 0.8172/v - 14.79/v^2)/(1 - 4.225/v + 4.87/v^2)$. The intrachain excluded volume force $\hat{\boldsymbol{F}}_i^{EV}$ is modeled with the soft potential used by Jendrejack et al.[32]

$$\hat{\boldsymbol{F}}_i^{EV} = -\sum_{j=1(j\neq i)}^{N_b} \frac{9}{2}\hat{\nu}^{ev,p}\left(\frac{3}{4\sqrt{\pi}}\right)^3 v^{9/2}\exp\left[-\frac{9}{4}v\hat{r}_{i,j}^2\right]\hat{\boldsymbol{r}}_{j,i} \tag{18}$$

where $\hat{\nu}^{ev,p} \equiv \nu^{ev,p}/{l_s}^3$ is the dimensionless form of the excluded volume parameter $\nu^{ev,p}$.

The interactions between a bead and the walls represented by $\hat{\boldsymbol{F}}_i^{EV,wall}$ are resolved using a modified Heyes−Melrose algorithm.[28,33] Whenever a bead moves outside the domain during a time step, it is moved to the nearest point on the domain boundary before commencing the next time step:

$$\Delta\hat{\boldsymbol{r}}_i^{HM} = \Delta\boldsymbol{p}_i H(\Delta p_i) \tag{19}$$

where $\Delta\hat{\boldsymbol{r}}_i^{HM}$ is the displacement vector due to the Heyes−Melrose algorithm, $\Delta\boldsymbol{p}_i$ is the vector pointing from the bead outside the domain to the nearest boundary point, and the Heaviside step function $H(\Delta p_i)$ restricts the application of the algorithm to only the beads that have penetrated the domain boundaries.

3.2. Parameters. Many different lengths of DNA were simulated in this study, ranging from $N_s = 10$ to $N_s = 300$. The chosen discretization of DNA was $v = 5.571$, which, assuming a persistence length of $A_p = 53$ nm, corresponds to DNA contour lengths of $L \approx 3$−90 μm. The excluded volume parameter was set to $\nu^{ev,p} = 3.71 \times 10^{-4}\,\mu m^3$ to accurately reproduce the unconfined radius of gyration of a T4-DNA molecule ($N_s = 254$ and $L = 75$ μm).

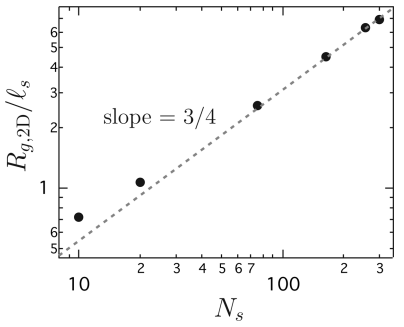

Figure 2. Plot of the 2D, in-plane radius of gyration $R_{g,2D}$ of chains at equilibrium in a 300 nm channel vs the chain length N_s. The predicted blob theory scaling $R_{g,2D} \sim N_s^{3/4}$ is also shown.

For the relaxation of initially extended molecules, the chains were uniformly stretched to the desired fractional extension (typically $X = 75\%$) along the x-direction and placed in the center of a 300 nm slit where the z-direction was transverse to the plane of the channel. The chains were then allowed to relax, and their configurations were saved for later analysis. Two different time steps were used. To obtain the short time behavior, a time step of $\Delta\hat{t} = 2 \times 10^{-5}$ was employed, and the chains were observed for a time of $\approx \tau_{II}$. For the long time behavior, a time step of $\Delta\hat{t} = 5 \times 10^{-4}$ was used, and the chains run for $\approx 10\tau_{II}$. For all measurements, at least 100 individual chains were simulated and averaged together for each chain length.

The equilibrium properties were obtained by initially placing the chains in the channel in a Gaussian manner and allowing them to equilibrate for $\approx 50\tau_{II}$. Configurations were then saved at specified time intervals for subsequent analysis. At least $\approx 300\tau_{II}$ worth of data was obtained.

4. Results

Before we begin analyzing the relaxation dynamics of confined chains, we would like to ascertain that we are using chains of adequate length for blob theory scalings to be valid. To do this, we look at the 2D, in-plane radius of gyration $R_{g,2D}$ of the chains at equilibrium. These results are shown in Figure 2, along with the predicted scaling of $R_{g,2D} \sim N_s^{3/4}$. It is clear that blob theory scalings are valid for chains with $N_s \geq 75$, and in our future analysis, we often only present results for these chain lengths.

In our study of the relaxation dynamics of confined chains, we first consider experimentally accessible measurables such as the relaxation of the longitudinal stretch at long times both at equilibrium and when initially perturbed away from equilibrium. This allows us to compare our findings to experimental results and validate our simulation model. We then look at the relaxation process in the transverse dimensions and attempt to build simple models based on Rouse-like chains to describe the observed dynamics. Finally, we consider how adding in additional physics, like intramolecular excluded volume and nonlinear springs, affects the relaxation dynamics.

4.1. Experimental Measurables. Typical measurables that are experimentally accessible are usually restricted to those involving the in-plane stretch of the molecule's major axis. We start by looking at the scaled longitudinal relaxation function $G_x(t) = \langle X(t)^2 \rangle - \langle X_{eq}{}^2 \rangle$, where $X(t)$ is the fractional extension in the longitudinal direction and X_{eq} is its average equilibrium value. Figure 3A shows a characteristic curve for $G_x(t)$ when the number of springs is $N_s = 164$. As seen in experiments, there are two distinct regions that are well-approximated by a single decaying exponential, each with a different time constant. The first region, with time constant τ_I, occurs at fractional extensions near $X = 30\%$ and represents the un-confined-like relaxation process where the chain

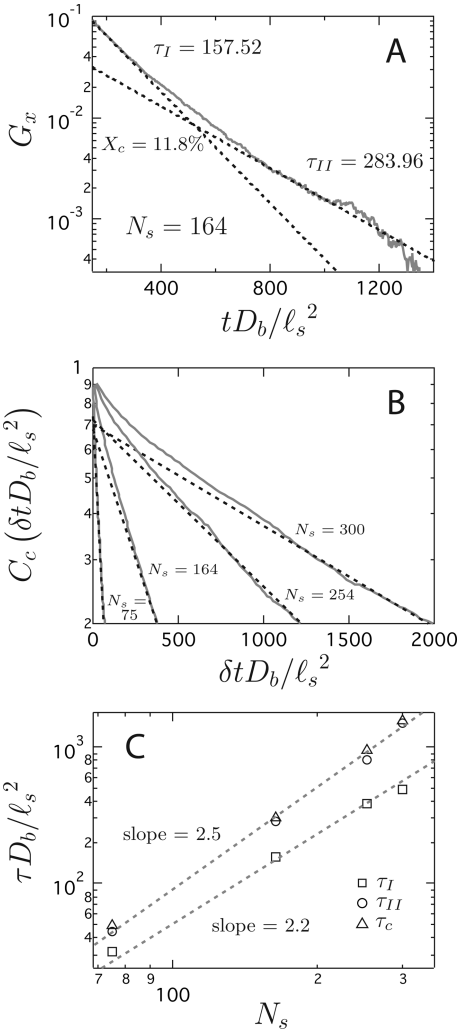

Figure 3. (A) Characteristic plot of the scaled longitudinal relaxation function $G_x(t) = \langle X(t)^2 \rangle - \langle X_{eq}{}^2 \rangle$ for chain length $N_s = 164$. The fittings for the two linear regions are also shown along with their respective time constants (τ_I and τ_{II}) and the predicted crossover extension X_c. (B) Plot of the equilibrium conformational autocorrelation function $C_c(\delta t)$ vs the lag time δt (see eq 20) for several chain lengths ($N_s = 75$, 164, 254, 300). The linear fittings for each curve are also shown. (C) Plot of various measured relaxation times vs chain length N_s. Included are the un-confined-like relaxation time τ_I, the near-equilibrium relaxation time τ_{II}, and the conformational relaxation time τ_c. Also shown are the predicted scalings $\tau_I \sim N_s^{2.2}$ and $\tau_{II} \sim \tau_c \sim N_s^{2.5}$.

is not sterically constrained. The second region occurs very near the chain's equilibrium size and, in agreement with experiments, has a longer time constant τ_{II} than the un-confined-like relaxation time ($\tau_{II} > \tau_I$). This second linear relaxation process is governed by the rearrangement of the blobs that compose the sterically confined chain. Finally, these two linear relaxation periods are connected by a non-linear transition region.

In Figure 3C, we have plotted both τ_I and τ_{II} as a function of chain length along with their predicted blob theory scalings. The simulation results for τ_{II} clearly follow the predicted scaling of $\tau_{II} \sim N_s^{2.5}$, while the results for τ_I appear to fall slightly below the theoretical scaling of $\tau_I \sim N_s^{2.2}$. The apparent discrepancy between the simulations and theory for τ_I is not unexpected and can be explained by noting that when eq 18 is used to account for EV, moderately extended chains are only mildly affected by the EV force. Because the un-confined-like relaxation time τ_I is seen near fractional extensions of $X \approx 30\%$, EV effects are not as significant as

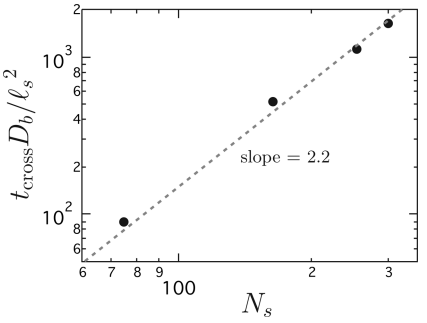

Figure 4. Plot of the computed crossover time t_{cross} vs chain length N_s. Also shown is the predicted scaling $t_{cross} \sim N_s^{2.2}$.

they are near the equilibrium extension. Therefore, the observed scaling for τ_I falls somewhere between the ideal chain scaling of $\sim N_s^2$ and the real chain scaling of $\sim N_s^{2.2}$.

Experiments have shown that relaxation processes measured when a confined molecule is at equilibrium should correspond to the second relaxation region where steric confinement is important. To confirm that our simulations can reproduce this finding, we considered the conformational relaxation time of a chain at equilibrium τ_c. The conformational autocorrelation function is defined as

$$C_c(\delta t) = \langle R_{ee}(t) \cdot R_{ee}(t+\delta t)\rangle / R_{ee,0}^2 \qquad (20)$$

where $R_{ee}(t)$ is the 2D, in-plane end-to-end vector of the chain, $R_{ee,0}$ is the equilibrium in-plane end-to-end distance, and δt is the lag time. The conformational autocorrelation functions for several different chain lengths are shown in Figure 3B along with their respective linear fittings, and the measured conformational relaxation times τ_c are plotted in Figure 3C. τ_c is very near the value of τ_{II} and follows the same predicted scaling $\tau_c \sim \tau_{II} \sim N_s^{2.5}$, in agreement with experiments.

We have clearly shown that our simulation model can reproduce the qualitative features seen in experiments. These include two distinct linear relaxation times for $G_x(t)$ with $\tau_{II} > \tau_I$, the proper scaling for τ_{II} with chain length, very near the predicted scaling for τ_I, and finally that near-equilibrium relaxation processes are associated with τ_{II}, as demonstrated by the fact that $\tau_c \sim \tau_{II}$.

One final experimentally accessible measurement we obtained is the time t_{cross} at which the crossover extension occurs. This is defined as the time where the two linear fittings for $G_x(t)$ intersect (see Figure 3A). Although t_{cross} can be found from experiments, to date this analysis has not been performed. t_{cross} is a measure of the when the transition between un-confined-like relaxation and near-equilibrium, sterically confined relaxation occurs. Based upon the current mechanisitic model of confined relaxation, the approach to this transition should be driven by the un-confined-like relaxation process leading up to it. Therefore, it is expected that t_{cross} should scale as $t_{cross} \sim \tau_I \sim N_s^{2.2}$. Indeed, this is clearly seen in Figure 4.

4.2. Transverse Dynamics. We now turn to the relaxation dynamics in the two transverse directions (y and z), which cannot currently be determined by experiments. Studying the of the out-of-plane behavior of these chains is particularly important because it can shed light on the physics of relaxation in confinement and help assess the validity of the current physical model.

4.2.1. General Features and Characteristics. We measured the 1D radius of gyration squared $R_{g,i}^2$ in the direction of each of the three coordinates (i can be either x, y, or z).

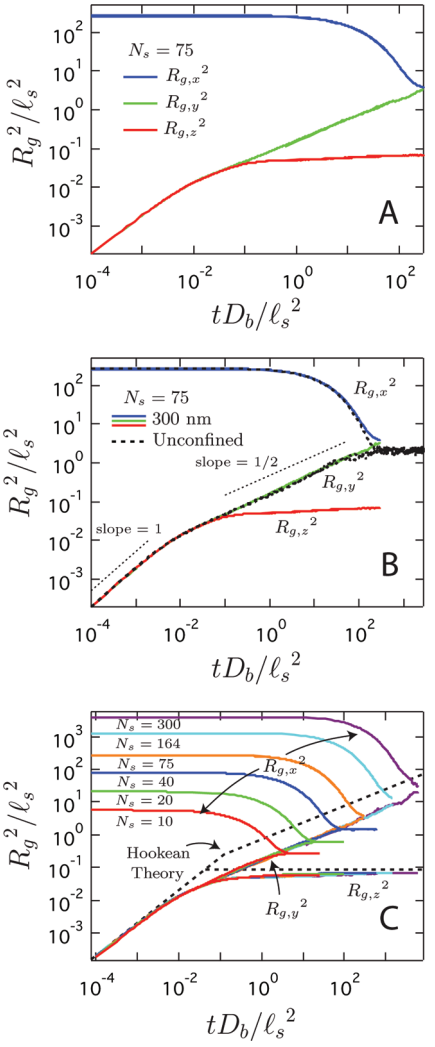

Figure 5. (A) Characteristic plot of the 1D radius of gyration squared in all three directions for a confined chain ($N_s = 75$ and $h = 300$ nm). (B) Plot of the 1D radius of gyration squared in all three directions for a single chain length ($N_s = 75$) both unconfined and in a 300 nm channel. The observed power law regions and their approximate scalings with time are also shown. (C) Plot of the 1D radius of gyration squared in all three directions for several chain lengths in a 300 nm channel. Also shown are the predicted values for each of the power law regimes as determined from the Hookean, Rouse-like theory given in eq 30.

Characteristic relaxation curves for all $R_{g,i}^2$ are shown in Figure 5A for a confined chain. In the longitudinal, or x-direction, $R_{g,x}^2$ remains fairly constant and slowly relaxes to its equilibrium value in an exponential manner only at long times. The behavior for the transverse directions is richer. $R_{g,y}^2$ and $R_{g,z}^2$, initially, are equal and grow together. However, at some point, the size of the chain in the confined dimension $R_{g,z}^2$ is restricted by the presence of the walls, and it peels off from the $R_{g,y}^2$ curve and quickly plateaus at its equilibrium value. On the other hand, the unconfined, transverse direction $R_{g,y}^2$ continues to grow even after $R_{g,z}^2$ has plateaued, and it finally reaches the same equilibrium value as the longitudinal direction so that at long times $R_{g,y}^2 = R_{g,x}^2$.

In Figure 5B, characteristic curves for unconfined relaxation have been added for comparison to the curves shown in Figure 5A for confined relaxation. In the unconfined case, $R_{g,y}^2$ and $R_{g,z}^2$ are always equivalent, all the way to their equilibrium. Additionally, at equilibrium all three directions have the same value so that $R_{g,x}^2 = R_{g,y}^2 = R_{g,z}^2 = R_{g,0}^2/3$. It is clear that, at short times, relaxation in all directions is the

same in both the confined and the unconfined cases. At intermediate times, $R_{g,z}^2$ plateaus for the confined case, while in the unconfined case it continues to grow, but the other two dimensions $R_{g,x}^2$ and $R_{g,y}^2$ continue to remain the same in both the confined and the unconfined cases. It is only at long times near equilibrium that $R_{g,x}^2$ and $R_{g,y}^2$ differ between the two cases. The unconfined chain has a smaller equilibrium value and it reaches this equilibrium sooner than the confined case. Lastly, two power law regimes are clearly see in the growth of the transverse directions $R_{g,y}^2$ and $R_{g,z}^2$ at short and intermediate times. The first regime is linear in time, while the second appears to follow a scaling close to $\sim t^{1/2}$. We will derive these scalings for a Rouse chain shortly.

Now that we have commented on the general features of the relaxation for a single chain, we look at the effect of chain length on the relaxation dynamics. In Figure 5C, we show the three 1D radii of gyration squared for several different chain lengths. As expected, $R_{g,x}^2$ is highly length dependent since its initial value is proportional to the chain length squared. Additionally, the relaxation times for the exponential decay and the final equilibrium values of $R_{g,x}^2$ are length dependent and have already been studied in section 4.1. On the other hand, the relaxation of the two transverse dimensions appears to change little based upon the length of the chain. $R_{g,z}^2$ nearly falls on a universal curve for all time and chain lengths, with only slight deviations which will be discussed later. $R_{g,y}^2$ also falls on a universal curve until it nears its equilibrium value, at which point it stops growing and plateaus at its length dependent final size.

Now that we have identified the general features of the relaxation process in the transverse dimensions, we turn to understanding the mechanisms behind the observed behavior. In particular, we would like to identify the important physics governing each of the observed power law regimes. And, with this in hand, we can study how the dynamics in the confined dimension affect, and are affected by, the longitudinal stretch.

4.2.2. Unconfined, Ideal Hookean Chain. Before we consider the relaxation dynamics in the confined dimension, we will look at the much simpler case of the transverse relaxation of an unconfined, Hookean chain. Because all three directions act independently for a linear chain, we only need to consider a 1D bead−spring chain with N_s springs each with a Hookean spring constant of H_s. Initially, the chain starts with all of the beads at the same point or, alternatively, with all of the springs having an initial stretch of zero. In this case, three different regimes arise during the relaxation process. We start by considering each of these from a scaling perspective and then use a continuous 1D Rouse model to prove some of our scalings and develop more quantitative expressions for the chain's size as a function of time.

At very short times, the bead movement is dominated by thermal forces. The springs are not yet extended enough to exert any significant force on the beads, so the beads act independently like an ideal gas. Therefore, the chain size initially grows in a diffusive manner such that $R_g^2 \sim D_b t$.

This growth continues until the spring forces are large enough to compete with the thermal forces. If this occurs when the spring lengths are of order l^*, then the spring forces are approximately $H_s l^*$ and the thermal forces are $k_B T/l^*$. Balancing these forces gives $l^* \sim (k_B T/H_s)^{1/2}$. At this point, the scaling of the chain size with time changes to a new power law $R_g^2 \sim At^\alpha$, where A and α will be determined below. Due to the influence of the significant spring forces, which impede the advancement of individual beads, the chain begins to grow subdiffusively so that $\alpha < 1$. We will refer to this new regime as the tension-dominated regime. The transition from the diffusive regime to the tension-dominated regime begins when R_g^2 is approximately $k_B T/H_s$, which occurs at $t \sim k_B T/H_s D_b$.

The third regime, which we call the equilibrium regime, occurs when the chain reaches its final size of $R_g^2 \sim N_s k_B T/H_s$. This should occur at times on the order of the longest Rouse relaxation time of the chain or $t \sim N_s^2 k_B T/H_s$. We can determine the power law exponent α and the scaling of the prefactor A for the tension-dominated regime by matching the end of the diffusive regime and the beginning of the equilibrium regime to the beginning and the end of the tension-dominated regime, respectively. Matching to the diffusive regime gives the expression $R_g^2 \sim k_B T/H_s \sim A(k_B T/H_s D_b)^\alpha$, and matching to the equilibrium regime gives $R_g^2 \sim N_s k_B T/H_s \sim A(N_s^2 k_B T/H_s D_b)^\alpha$. This only holds valid for $\alpha = 1/2$ and $A \sim (kBTD_b/H_s)^{1/2}$. Combining all of our results, we finally arrive at a scaling for the chain size in all three regimes as a function of time

$$R_g^2 \sim \begin{cases} D_b t, & t \ll \dfrac{k_B T}{H_s D_b} \\ \left(\dfrac{k_B T D_b}{H_s}\, t\right)^{1/2}, & \dfrac{k_B T}{H_s D_b} \ll t \ll \dfrac{N_s^2 k_B T}{H_s D_b} \\ \dfrac{N_s k_B T}{H_s}, & t \gg \dfrac{N_s^2 k_B T}{H_s D_b} \end{cases} \quad (21)$$

To more rigorously confirm our scalings, particularly in the tension-dominated regime, we now briefly develop a continuous 1D Rouse model for the transverse relaxation of an initially straight chain. Lengthier more detailed derivations are available elsewhere.[19,34] We start with a discrete bead−spring chain with N_b beads connected by $N_s = N_b - 1$ Hookean springs with spring constant H_s. If we allow the nth bead position to be a continuous variable, we can recast the discrete bead−spring model as a continuous chain obeying the partial differential equation

$$\zeta_b \frac{\partial r_n}{\partial t} = H_s \frac{\partial^2 r_n}{\partial n^2} + F_n^B \quad (22)$$

where the second moment of the Brownian force is

$$\langle F_n^B(t) \rangle = 0$$
$$\langle F_n^B(t) F_m^B(t') \rangle = 2k_B T \zeta_b \delta(n-m)\delta(t-t') \quad (23)$$

The initial condition and boundary conditions are given by

$$r_n|_{t=0} = \left.\frac{\partial r_n}{\partial n}\right|_{n=0} = \left.\frac{\partial r_n}{\partial n}\right|_{n=N_b} = 0 \quad (24)$$

The normal coordinates of the system can be found by solving the eigenvalue problem.

We are interested in the chain's ensemble-averaged radius of gyration squared

$$\langle R_g^2(t) \rangle = \left\langle \frac{1}{N_b} \int_0^{N_b} dn [r_n(t) - R_{c.m.}(t)]^2 \right\rangle \quad (25)$$

where $R_{c.m.}(t)$ is the center of mass of the chain. Using normal coordinates and linear response theory, it can be shown that

$$\langle R_g^2(t) \rangle = \frac{N_b k_B T}{\pi^2 H_s} \sum_{p=1}^{\infty} p^{-2} \left[1 - \exp\left(\frac{-2\pi^2 H_s p^2}{N_b^2 \zeta_b} t\right)\right] \quad (26)$$

At long times, the exponential dies off, and only the sum $\sum_{p=1}^{\infty} p^{-2} = \pi^2/6$ remains. This gives an equilibrium value of

$\langle R_g{}^2(t)\rangle = N_b k_B T/6H_s$, which is exactly the expected theoretical result.

If we transform the summation $\sum_{p=1}^{\infty}$ in eq 26 to an integral $\int_{6/\pi}^{\infty} dp$ (the lower bound has been chosen so that the equilibrium value remains the same) then our expression becomes

$$\langle R_g{}^2(t)\rangle = \frac{N_b k_B T}{6H_s}\left[1 - \exp\left(\frac{-72H_s}{\pi^2 N_b{}^2 \zeta_b} t\right) + \sqrt{\frac{72H_s}{\pi N_b{}^2 \zeta_b} t}\,\mathrm{erfc}\left(\sqrt{\frac{72H_s}{\pi^2 N_s{}^2 \zeta_b} t}\right)\right] \quad (27)$$

Finally, since we are interested in short times (i.e., $t \ll \pi^2 N_b{}^2 \zeta_b/72H_s$), we can expand this expression into a power series and keep only the leading order term

$$\langle R_g{}^2(t)\rangle = \sqrt{\frac{2k_B T D_b}{\pi H_s} t} \quad (28)$$

As predicted by our previous scaling arguments, in the tension-dominated regime $R_g{}^2 \sim t^{1/2}$.

For the diffusion-dominated regime, $R_g{}^2$ is simply the mean-squared displacement of a gas of beads that all initially start at the same point. This gives the well-known result $R_g{}^2 = 2D_b t$.

If we take all of our results, we can determine the locations of the regime transitions from the intersections of the expressions. Finally, combining all of our findings, we find

$$R_g{}^2 \approx \begin{cases} 2D_b t, & t \ll \dfrac{k_B T}{H_s D_b} \\ \left(\dfrac{2k_B T D_b}{\pi H_s} t\right)^{1/2}, & \dfrac{k_B T}{H_s D_b} \ll t \ll \dfrac{N_s{}^2 k_B T}{H_s D_b} \\ \dfrac{N_s k_B T}{6H_s}, & t \gg \dfrac{N_s{}^2 k_B T}{H_s D_b} \end{cases} \quad (29)$$

Comparing this to eq 21, we find that our predicted scalings are, indeed, correct.

Our theoretical predictions for the two power law regimes of the unconfined case are plotted in Figure 5C to be compared to $R_{g,y}{}^2$. It is clear that our expression catches the qualitative behavior seen in the simulations. It quantitatively predicts the value in the diffusive regime at short times, but it overestimates the time at which the transition to the tension-dominated regime occurs. This leads to an overprediction of $R_{g,y}{}^2$ in the tension-dominated regime. These discrepancies are due to the nonlinearities in the spring law used in the simulations when the chain is initially stretched beyond its linear regime. Effectively, this increases the spring constant H_s felt by the beads which, according to eq 29, should decrease the time of the transition to the tension-dominated regime as well as the value of $R_{g,y}{}^2$ in this regime. So incorporating the spring law nonlinearities into the above Hookean analysis should bring the theoretical prediction more in line with the simulation results. The effects of these nonlinearities will be discussed in greater detail later.

4.2.3. Confined, Ideal Hookean Chain. When a Hookean chain relaxes in a channel of height $h \ll (N_s k_B T/H_s)^{1/2}$, the equilibrium size of the chain in the confined dimension decreases to $R_g{}^2 \sim h^2$. Going further, if we assume that the bead distribution across the channel height is uniform, then $R_g{}^2 = h^2/12$. This is actually an overprediction of $R_g{}^2$ because the bead distribution is not truly uniform and has a Gaussian quality to it.

Assuming that $h \gg (k_B T/H_s)^{1/2}$, the effect of confinement is both to limit the chain size and to truncate the width of the tension-dominated regime so that

$$R_g{}^2 \approx \begin{cases} 2D_b t, & t \ll \dfrac{k_B T}{H_s D_b} \\ \left(\dfrac{2k_B T D_b}{\pi H_s} t\right)^{1/2}, & \dfrac{k_B T}{H_s D_b} \ll t \ll \dfrac{\pi H_s h^4}{288 k_B T D_b} \\ \dfrac{h^2}{12}, & t \gg \dfrac{\pi H_s h^4}{288 k_B T D_b} \end{cases} \quad (30)$$

A similar expression can be written if $h \ll (k_B T/H_s)^{1/2}$, but in that case, the diffusive regime is truncated and the tension-dominated regime is eliminated entirely.

This prediction for the confined case is also plotted in Figure 5C to be compared to $R_{g,z}{}^2$. Again, fairly good qualitative agreement exists between theory and simulations except that the tension-dominated regime is not seen in the theoretical prediction, as $h \ll (k_B T/H_s)^{1/2}$, but it is present in the simulation results. As in the unconfined case, this is due to the nonlinearities in the spring law.

4.2.4. Excluded Volume. As mentioned in section 4.1, the EV forces are not significant for moderately stretched chains. This means that the effects of EV will not be seen until the chain has relaxed significantly in the longitudinal direction, which only occurs on time scales on the order of τ_I or longer. This can clearly be seen in Figure 6 where the curves for the chain with EV do not deviate from those without EV until very near equilibrium. Therefore, the effects of EV on the transverse dynamics are minimal except at very long times.

We can demonstrate this by considering a scaling analysis to estimate the fractional extension X_{ev} at which EV becomes important. We accomplish this using a Flory-type approach where an estimate of the energy gain due to excluded volume interactions F_I is obtained using a mean field approach (see Chapter 3 of Rubinstein and Colby[27] for more details concerning the following analysis). We begin by viewing the chain as a series of tension blobs whose in-plane dimensions are ξ_y and whose transverse dimensions are h (i.e., they are small disks). Therefore, the pervaded volume of a tension blob scales as $\sim h\xi_y{}^2$. If there are g_y Kuhn lengths in a blob, then the chain interaction parameter[27] of a blob is given by

$$z \sim \frac{F_I}{k_B T} \sim \nu^{ev,p}\frac{g_y{}^2}{h\xi_y{}^2} \sim \frac{\nu^{ev,p}}{hb_K{}^2} g_y \quad (31)$$

where here F_I is the energy gain for a blob and $\nu^{ev,p}$ is the excluded volume parameter for a Kuhn length. The last scaling comes from assuming ideal chain statistics within a blob, as Flory did (i.e., $\xi_y \sim g_y{}^{1/2} b_K$). The chain interaction parameter simply compares the energy gain due to excluded volume interactions to the thermal energy, so the point at which EV becomes important is when $z \approx 1$. Therefore, the critical number of Kuhn lengths in a tension blob $g_{y,ev}$, where EV becomes important is

$$g_{y,ev} \sim \frac{hb_K{}^2}{\nu^{ev,p}} \quad (32)$$

which corresponds to a fractional extension of

$$X_{ev} \sim \frac{(N_K/g_{y,ev})\xi_{y,ev}}{N_K b_K} \sim g_{y,ev}{}^{-1/2} \sim \sqrt{\frac{\nu^{ev,p}}{hb_K{}^2}} \quad (33)$$

For our choice of parameters, in a 300 nm channel, this corresponds to a fractional extension of $X_{ev} \approx 0.3$. Of course,

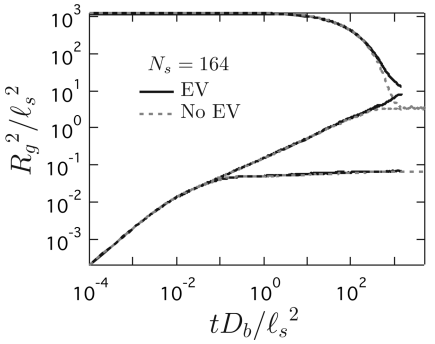

Figure 6. Plot of the 1D radius of gyration squared in all three directions for a single chain length of $N_s = 164$ both with and without EV. The initial stretch of the chain was 75% in a 300 nm channel.

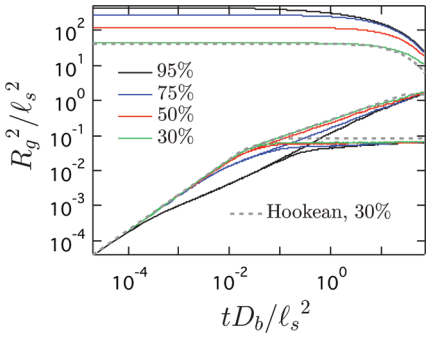

Figure 7. Plot of the 1D radius of gyration squared in all three directions for a single chain length of $N_s = 75$ in a 300 nm channel. The results for various values of the initial fractional extension are shown. Also included is the Hookean theory given by eqs 29 and 30.

this is a scaling analysis, so order unity prefactors have been ignored. But this suggests that a chain must relax significantly in the longitudinal direction before EV effects become important, and this only occurs at very long times. This means that examining chain growth across multiple time scales by plotting the chain size against a logarithmic scale of time is inappropriate for the study of the effects of EV. To see these effects, a linear time scale must be used, which is precisely the sort of analysis performed in section 4.1.

EV does not directly affect the dynamics of the confined dimension, even at long time scales, as will be shown in the following section. However, we will show that under certain conditions spring nonlinearities can lead to coupling between the confined and longitudinal dimensions that affects the relaxation of $R_{g,z}^2$ to its true equilibrium value at long times. Therefore, $R_{g,z}^2$ is sensitive to EV insofar as the longitudinal dimension is affected by EV at long times. On the other hand, the unconfined, transverse dimension certainly feels the effects of EV as it nears the equilibrium value it shares with the longitudinal dimension, but at this point, these two unconfined dimensions are governed by the same linear relaxation processes which have already been studied in significant detail in section 4.1. So no further analysis is required.

4.2.5. Nonlinearities. Finally, we consider the effects of the spring nonlinearities, which are most evident at the beginning of the relaxation process when the springs are highly stretched. One consequence of these nonlinearities is that the spring force is no longer independent for each dimension. This means that the strong stretching in the longitudinal direction leads to an increased effective spring constant in both of the transverse directions. As already pointed out in sections 4.2.2 and 4.2.3, this can lead to deviations from the

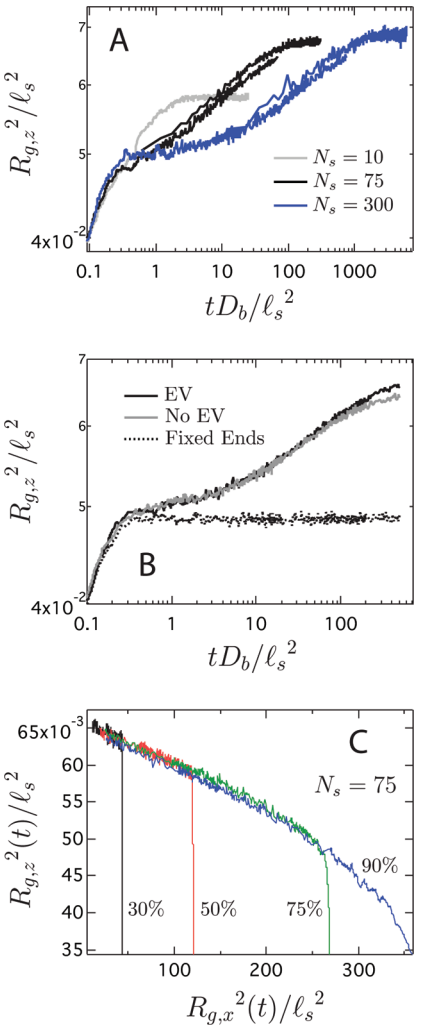

Figure 8. (A) Plot of 1D radius of gyration squared in the confined, transverse dimension $R_{g,z}^2$ for several different chain lengths in a 300 nm channel with an initial fractional extension of 75%. Only the equilibrium regime is shown (see Figure 5C for the entire relaxation process). Two curves are seen for $N_s = 75$ and 300 because the data from both the short time and long time simulations are plotted. (B) Plot of 1D radius of gyration squared in the confined, transverse dimension $R_{g,z}^2$ for a single chain length of $N_s = 75$ in a 300 nm channel with an initial fractional extension of 75%. The results for three different cases are shown: with EV, without EV, and the longitudinal stretch held fixed. Only the equilibrium regime is shown. (C) Plot of 1D radius of gyration squared in the confined, transverse dimension $R_{g,z}^2$ vs the 1D radius of gyration squared in the longitudinal dimension $R_{g,x}^2$ for a single chain length of $N_s = 75$ in a 300 nm channel. The results for several different initial fractional extensions is shown.

Hookean theory and retards the growth of the transverse dimensions during the tension-dominated regime.

To clearly demonstrate this effect, we simulated the relaxation of a chain from several different initial fractional extensions. The results are shown in Figure 7. It has been observed that chains behave in a Hookean manner up to fractional extensions around 30%. In accordance with this, excellent agreement is seen between the Hookean theory and the chain initially stretched to 30%. As the initial extension is increased, the size in the transverse dimensions falls farther below that of the theory. This is precisely the expected effect of the strong nonlinearities in the springs at high extensions.

The nonlinearities also affect the equilibrium regime of the confined, transverse dimension. Figure 8A shows a zoomed in view of $R_{g,z}^2$ from Figure 5C for several different chain

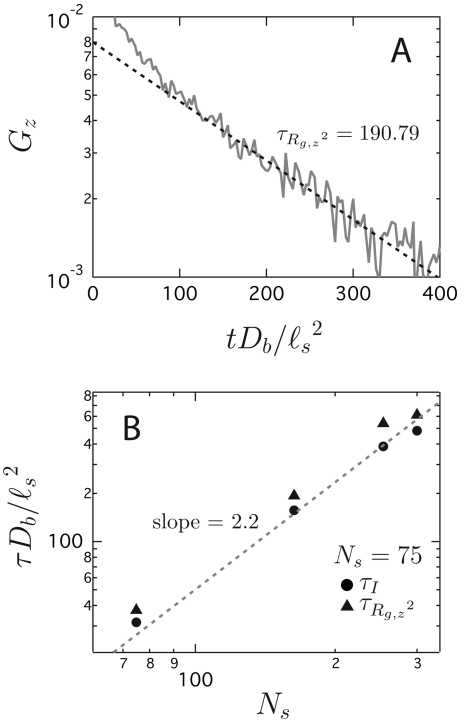

Figure 9. (A) Characteristic plot of the confined transverse relaxation function $G_z(t) = [R_{g,z,0}^2 - R_{g,z,0}^2]/l_s^2$ for chain length $N_s = 164$. The fitting for the linear region is shown. (B) Plot of the un-confined-like relaxation times τ_I and $\tau_{R_{g,z}^2}$ vs chain length N_s. Also shown is the predicted scaling $\tau_{R_{g,z}^2} \sim \tau_I \sim N_s^{2.2}$.

lengths. We have zoomed in on the region that looks like a plateau in Figure 5C, which we have been referring to as the equilibrium regime. In Figure 8A, $R_{g,z}^2$ is the same for all three chain lengths through the diffusive and tension-dominated regimes, but they behave somewhat differently once they reach the equilibrium regime. (Note that the two curves seen for both $N_s = 75$ and 300 are due to the inclusion of both the short time and long time simulations.) The Hookean theory of section 4.2.3 predicts that $R_{g,z}^2$ should immediately plateau to its final equilibrium value after the tension-dominated regime, but clearly the dynamics are richer for real chains. All three chain lengths exit the tension-dominated regime by temporarily pausing their growth of $R_{g,z}^2$ at an intermediate value slightly below their final equilibrium. The duration of this pause is dependent upon the chain length. For $N_s = 10$, the pause is only barely evident, while it is quite significant for $N_s = 300$. After this interruption in its growth, $R_{g,z}^2$ slowly approaches its final value.

To prove that this behavior is due to the spring nonlinearities, we ran a simulation where an initially stretched chain was allowed to relax in the transverse directions, but its initial longitudinal stretch was held fixed for all time. The result is shown in Figure 8B along with the results for chains with and without EV that are allowed to relax in the longitudinal direction. The two chains that are allowed to relax in all dimensions are nearly identical except that the chain with EV has a slightly higher final equilibrium value at long times. Therefore, EV cannot account for this behavior. On the other hand, the chain whose stretch is held fixed plateaus at its final value precisely where the other chains temporarily pause. Clearly, this temporary arrest in the growth is due to the nonlinearities of the springs, and the subsequent slow approach to equilibrium is due to the relaxation of the longitudinal stretch which reduces the tension in the springs.

To demonstrate that relaxation of the longitudinal stretch is responsible for the slow approach to equilibrium after the pause, we have taken the data from Figure 7 and plotted $R_{g,z}^2$ against $R_{g,x}^2$. This is shown in Figure 8C for different initial chain extensions. Initially, $R_{g,z}^2$ grows during the diffusive and tension-dominated regimes without much change in $R_{g,x}^2$, which relaxes on much longer time scales. But once the equilibrium regime is reached, all the curves fall on the same universal curve. This reveals that a quasi-steady equilibrium exists for $R_{g,z}^2$ during the equilibrium regime and it is slaved to the relaxation of the longitudinal stretch. This also verifies the quasi-steady assumption made in the tension-blob physical model for the relaxation, as discussed in section 2.2.2.

A consequence of this quasi-steady equilibrium is that during the equilibrium regime, $R_{g,z}^2$ is a measure of the relaxation of the longitudinal stretch. This means analyzing $R_{g,z}^2$ provides another way of studying the relaxation times of the chain. We can do this by defining a relaxation function $G_z(t) = [R_{g,z,0}^2 - R_{g,z,0}^2]/l_s^2$ for the confined dimension. A characteristic curve for $G_z(t)$ is shown in Figure 9A. An obvious linear region is seen, indicative of a single exponential decay with the time constant $\tau_{R_{g,z}^2}$. Because this approach to equilibrium is due the nonlinearities in the spring law when the longitudinal direction is extended beyond 30%, it is expected that $\tau_{R_{g,z}^2}$ should provide an estimate of the un-confined-like relaxation time τ_I. Indeed, good agreement is found between the two as seen in Figure 9B, and it is clear that they follow the same scaling $\tau_{R_{g,z}^2} \sim \tau_I \sim N_s^{2.2}$.

5. Conclusions

We have used Brownian dynamics simulations to study the relaxation of initially stretched chains in slitlike confinement. We have shown that our simulation technique is capable of reproducing the qualitative findings of recent experimental studies. In particular, our simulations clearly show the existence of two distinct relaxation times in the linear force regime: one that scales similar to an un-confined-like relaxation time and another that follows the scalings predicted by blob theory. We have conclusively demonstrated that the emergence of the second relaxation time is due to excluded volume effects and not hydrodynamic interactions.

We developed a Rouse-like theory to describe the confined relaxation of the transverse dimensions of an initially straight bead−spring chain and find good agreement between our theory and the simulations. The effects of excluded volume and spring nonlinearities on the dynamics were also explored. It was found that these nonlinearities lead to a quasi-steady equilibrium between the size of the chain in the confined dimension and in the longitudinal dimension. This corroborates one of the underlying assumptions of the physical model for confined relaxation proposed by Balducci and co-workers.[10]

Our results are important to developing a clear mechanistic understanding of the relaxation of polymers in slitlike confinement. Not only is this a problem of fundamental importance in polymer physics, it also has practical interest for the development of microfluidic devices that exploit confinement to manipulate DNA molecules. This work only considered the scalings of the relaxation times with chain length, and the height of the channel was not varied. Future studies should examine the predicted scalings of the relaxation times with channel height. Additionally, hydrodynamics interactions were not included in the simulation model, and their effects should be explored at a later date.

Acknowledgment. The authors are indebted to Jing Tang and Will Uspal for their numerous insightful discussions. Additionally, the authors thank the Singapore-MIT Alliance for Research

and Technology (SMART) for funding, and the National Science Foundation Grant CBET-0852235.

References and Notes

(1) Doyle, P. S.; Bibette, J.; Bancaud, A.; Viovy, J.-L. *Science* **2002**, *295*, 2237.
(2) Han, J.; Craighead, H. G. *Science* **2000**, *288*, 1026.
(3) Chan, E. Y.; Goncalves, N. M.; Haeusler, R. A.; Hatch, A. J.; Larson, J. W.; Maletta, A. M.; Yantz, G. R.; Carstea, E. D.; Fuchs, M.; Wong, G. G.; Gullans, S. R.; Gilmanshin, R. *Genome Res.* **2004**, *14*, 1137.
(4) Jo, K.; Dhingra, D. M.; Odijk, T.; de Pablo, J. J.; Graham, M. D.; Runnheim, R.; Forrest, D.; Schwartz, D. C. *Proc. Natl. Acad. Sci. U.S.A.* **2007**, *104*, 2673.
(5) Perkins, T. T.; Quake, S. R.; Smith, D. E.; Chu, S. *Science* **1994**, *264*, 822.
(6) Bakajin, O. B.; Duke, T. A. J.; Chou, C. F.; Chan, S. S.; Austin, R. H.; Cox, E. C. *Phys. Rev. Lett.* **1998**, *80*, 2737.
(7) Turner, S.; Cabodi, M.; Craighead, H. *Phys. Rev. Lett.* **2002**, *88*, 128103.
(8) Schroeder, C. M.; Babcock, H. P.; Shaqfeh, E. S. G.; Chu, S. *Science* **2003**, *301*, 1515.
(9) Reisner, W.; Morton, K. J.; Riehn, R.; Wang, Y. M.; Yu, Z.; Rosen, M.; Sturm, J. C.; Chou, S. Y.; Frey, E.; Austin, R. H. *Phys. Rev. Lett.* **2005**, *94*, 196101.
(10) Balducci, A.; Hsieh, C.-C.; Doyle, P. S. *Phys. Rev. Lett.* **2007**, *99*, 238102.
(11) Bonthuis, D. J.; Meyer, C.; Stein, D.; Dekker, C. *Phys. Rev. Lett.* **2008**, *101*, 108303.
(12) Reccius, C. H.; Mannion, J. T.; Cross, J. D.; Craighead, H. G. *Phys. Rev. Lett.* **2005**, *95*, 268101.
(13) Hsieh, C.-C.; Balducci, A.; Doyle, P. S. *Macromolecules* **2007**, *40*, 5196.
(14) Balducci, A.; Doyle, P. S. *Macromolecules* **2008**, *41*, 5485.
(15) Fisher, J. K.; Ballenger, M.; O'Brien, E. T.; Haase, J.; Superfine, R.; Bloom, K. *Proc. Natl. Acad. Sci. U.S.A.* **2009**, *106*, 9250.
(16) Grassia, P.; Hinch, E. J. *J. Fluid Mech.* **1996**, *308*, 255.
(17) Doyle, P. S.; Shaqfeh, E. S. G.; McKinley, G. H.; Spiegelberg, S. H. *J. Non-Newtonian Fluid Mech.* **1998**, *76*, 94.
(18) Dimitrakopoulos, P. *J. Fluid Mech.* **2004**, *513*, 265.
(19) Doi, M.; Edwards, S. *The Theory of Polymer Dynamics*; Oxford University Press: New York, 1986.
(20) Milchev, A.; Binder, K. *J. Phys. II* (*France*) **1996**, *6*, 21.
(21) Hagita, K.; Koseki, S.; Takano, H. *J. Phys. Soc. Jpn.* **1999**, *68*, 2144.
(22) Stigter, D. *Biophys. Chem.* **2002**, *101*, 447.
(23) Woo, N. J.; Shaqfeh, E. S. G.; Khomami, B. *J. Rheol.* **2004**, *48*, 281.
(24) Brochard, F. *J. Phys.* (*Paris*) **1977**, *38*, 1285.
(25) Tang, J.; Trahan, D. W.; Doyle, P. S. *Macromolecules* **2010**, *43*, 3081.
(26) Daoud, M.; de Gennes, P. G. *J. Phys.* (*Paris*) **1977**, *38*, 85.
(27) Rubinstein, M.; Colby, R. H. *Polymer Physics*; Oxford University Press: New York, 2003.
(28) Kim, J. M.; Doyle, P. S. *J. Chem. Phys.* **2006**, *125*, 074906.
(29) Underhill, P. T.; Doyle, P. S. *J. Rheol.* **2006**, *50*, 513.
(30) Marko, J. F.; Siggia, E. D. *Macromolecules* **1995**, *28*, 8759.
(31) Underhill, P. T.; Doyle, P. S. *J. Non-Newtonian Fluid Mech.* **2004**, *122*, 3.
(32) Jendrejack, R. M.; de Pablo, J. J.; Graham, M. D. *J. Chem. Phys.* **2002**, *116*, 7752.
(33) Heyes, D.; Melrose, J. *J. Non-Newtonian Fluid Mech.* **1993**, *46*, 1.
(34) Trahan, D. W. Simulating DNA Behavior in Microfluidic Devices. *Ph.D. Thesis*, Massachusetts Institute of Technology, 2010.